Evaluation of Burden Descent Model for Burden Distribution in Blast Furnace

Ping ZHOU[1],   Peng-yu SHI[1],   Yan-po SONG[1],   Kai-le TANG[1],
Dong FU[2],   Chenn Q. ZHOU[1,2]

(1. School of Energy Science and Engineering, Central South University, Changsha 410083, Hunan, China;   2. Center for Innovation through Visualization and Simulation, Purdue University Calumet, Hammond 46323, Indiana, USA)

Abstract: Mathematical models for burden descending process have been applied to obtain whole burden structures in blast furnace, whereas the accuracy of those burden descent models has not been sufficiently investigated. Special evaluation method based on timeline burden profiles was established to quantitatively evaluate the error between experimental and modeled burden structures. Four existing burden descent models were utilized to describe the burden structure of a 1/20 scaled warm blast furnace. Input modeling conditions including initial burden profile, descending volumes in each time interval, and normalized descending velocity distribution were determined via special image processing technology. Modeled burden structures were evaluated combined with the published experimental data. It is found that all the models caught the main profile of the burden structure. Furthermore, the improved nonuniform descent model (Model IV) shows the highest level of precision especially when burden descends with unstable velocity distribution tendency. Meanwhile, the traditional nonuniform descent model (Model III) may also be desirable to model the burden descending process when the burden descending velocity presents a linear tendency. Finally, the uniform descent model (Model I) might be the first option for roughly predicting burden structure.

Key words: blast furnace; burden distribution; mathematical model; burden descent model; evaluation

Blast furnace (BF) is a vertical reactor with the countercurrent flows between solids and gases for reducing iron oxides to iron. The efficiency of BF is dominated by the heat exchange between gas and charged materials, but essentially depends on the gas flow distribution[1]. Due to differences in permeability and density of the charged materials, the gas flow distribution is largely controlled by the burden distribution[2,3]. Besides, the control of radial ore/coke ratio distribution is significant in forming the gas passage and resultant gas permeability in the furnace operation[4,5]. Thus, many mathematical models have been established to simulate the burden distribution in BF[6-21]. Among those studies, the movement processes of the raw materials simplified in the mathematical model mainly include: discharging from the hopper, colliding on the chute, sliding along the chute with the driven force of gravity, centrifugal force, reaction force, friction force and

Coriolis force, falling in the freeboard driven by gravity, buoyancy force and drag force, stocking on the previous burden to form a new burden profile, and descending to form the entire burden structure.

The mechanism of the burden descent sub-model is crucial for making accurate burden structure prediction since it is a direct reflection of the BF's internal condition. The continuous descending theory, assuming that the physical properties of the material remain uniform throughout the whole descending process, is made to develop analytical burden descent models based on empirical data[9]. Over the past few decades, continuous models have gained wide applications ranging from accurate prediction of the burden structure[9-12] to fast evaluation of the charging programs[13] in running industrial BF.

Nishio and Ariyama[14] derived the original analytical burden descent model in 1982. With the assumption of radial descending path and uniform de-

scending speed, whole layer structures could be obtained from the top burden profile. Ichida et al. [15] investigated the influence of shaft expansion on burden descending path via a scaled cold model. The corresponding study divided the shaft region into two parts, the vertical descending region and the radial descending region. The latter was proved to be the only affected region through comparison of the measured particle stream lines in both regions. Besides, the operation condition of the BF strongly influenced burden descending velocity along the radius. With linearity assumption on the distribution of vertical descending velocity, the non-uniform descent model was proposed by Kajiwara et al. [16] according to the operating furnace measurement on Kokura BF No. 2. In addition, the distribution of vertical descending velocity can also be significantly affected by the charging pattern. Experiment data of the 1/20 scaled warm model built by Ichida et al. [17] showed that strong nonlinear descending velocity distribution might occur even under normal charging pattern. In recent years, with the development of measurement technology on top burden surface[18], radial descending velocity distribution of the top burden surface could be measured entirely and accurately by equipments such as laser scanner and multiradar. Burden descent models based on entire velocity distribution of the top layer have gained wide range of applications on burden structure prediction[19].

Due to the harsh in-furnace condition, it is difficult to measure burden profile of each layer below the top burden surface with traditional equipments. Validations of those burden descent models are mainly conducted on scaled cold models which neglected the chemical reactions[2,5,15]. However, the local solid consumption, i. e. ore reduction and coke

gasification, plays a critical role in burden descending process. Accuracy of those burden descent models has not been sufficiently investigated. The objective of this study was to evaluate the suitability of the burden descent models and to analyze their accuracy through comparison with published experimental data of a scaled warm BF[17].

1 Burden Descent Models

The burden descent models, by which the burden layers are shifted downwards, are based on the assumption that the physical properties of the materials remain uniform throughout the whole descending process. The influence of the shaft expanding along the vertical direction has also been taken into account while the effects like mixed layer formation and gas flow are neglected.

The concepts of the four conventional burden descent models are shown in Fig. 1. In model I[14] (Fig. 1(a)), the burden descends along the lines radiating from the cone apex O located above the tapered wall. O is the intersection of the furnace centerline and the extension of the furnace shaft. The basic assumption of model I is that particles in the same level possess the identical vertical descending velocities which results in a uniform vertical advancement for these particles. In a blast furnace with throat radius R, throat height y_0 and shaft angle α_1, the movement of the particles from the point (x, y) to the point (x', y') in the stack region is formulated as Eq. (1).

$$\begin{cases} y' = [3V_d/(\pi\tan^2\alpha_1) + (y - y_0 + \\ \quad R/\tan\alpha_1)^3]^{1/3} + y_0 - R/\tan\alpha_1 \\ x' = x(y' - y_0 + R/\tan\alpha_1)/(y - y_0 + \\ \quad R/\tan\alpha_1) \end{cases} \quad (1)$$

where, V_d is the descending volume enclosed by the

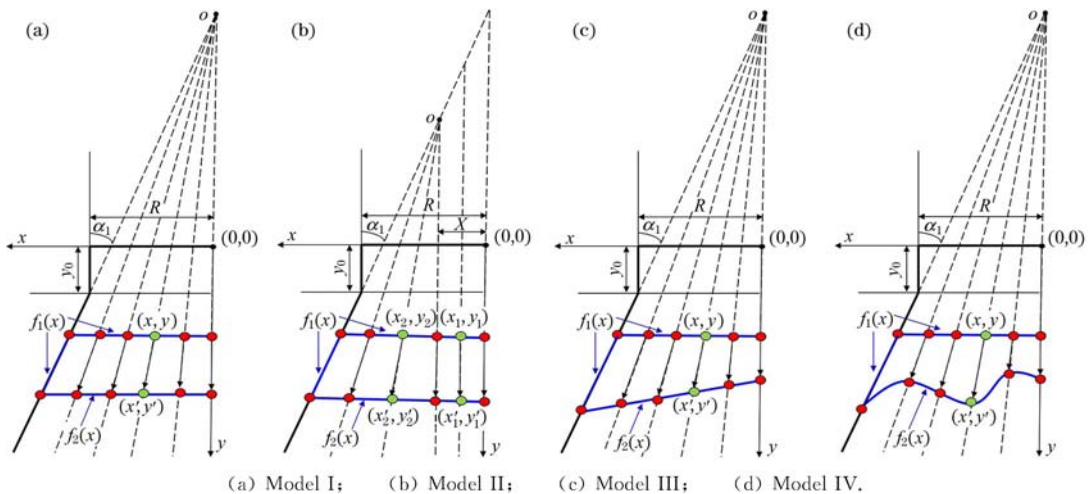(a) Model I;   (b) Model II;   (c) Model III;   (d) Model IV.

Fig. 1   Illustration of different burden descent models

initial burden profile $f_1(x)$ and the final burden profile $f_2(x)$, m^3.

As for model II[15], shaft expanding along the vertical direction affects only the peripheral region $(x > X)$. Raw materials in this region descend along the lines radiating from the new cone apex O which is the intersection of the vertical line $(x = X)$ and the extension of the furnace shaft. While in the center region $(x \leqslant X)$, the burden descends vertically. The radial distribution of the vertical burden descending velocities in the same level is assumed to be equal, which is virtually identical to model I. The movement of particles from the point (x_1, y_1) and (x_2, y_2) to the point (x_1', y_1') and (x_2', y_2') in the stack region $(x_1 \leqslant X, x_2 > X, y_1 = y_2 = y)$ is formulated as Eq. (2).

$$
\begin{cases}
y_1' = y_2' = [3V_d/(\pi\tan^2\alpha_1) + (y - y_0 + \\
\quad R/\tan\alpha_1)^3]^{1/3} + y_0 - R/\tan\alpha_1 \\
x_1' = x_1 \\
x_2' = (x_2 - X)(y_2' - y_0 + R/\tan\alpha_1)/(y_2 - \\
\quad y_0 + R/\tan\alpha_1) + X
\end{cases} \tag{2}
$$

Burden descending trajectories in model III[16] (Fig. 1(c)) and model IV[19] (Fig. 1(d)) are the same as that in model I. With linearity assumption on the distribution of vertical descending velocities $v_y(x)$ (Eq. (3)), the leveled initial profile in model III becomes tilted via certain amount of burden descending. While in model IV, $v_y(x)$ is entirely determined by the experimental result which is generally conducted by laser scanner and multiradar. Therefore, in model IV, $v_y(x)$ is an implicit func-

tion depending on the variable x. Except for the difference on the determination of $v_y(x)$, formulations for the movement of particles in model III and model IV can be expressed in the same way as shown in Eq. (4).

$$
v_y(x) = kx + c \tag{3}
$$

$$
\begin{cases}
y' = y + v_y(x) \cdot \Delta t \\
x' = x(y' - y_0 + R/\tan\alpha_1)/(y - \\
\quad y_0 + R/\tan\alpha_1) \\
|\int_0^{x_{max}} 2\pi x[f_1(x) - f_2(x)]dx - V_d|/ \\
\quad V_d \leqslant \varepsilon
\end{cases} \tag{4}
$$

where, k represents the linear coefficient between $v_y(x)$ and x, s^{-1}; c is an constant, m $\cdot$ s^{-1}; Δt represents the step time of each advancement, s; and ε is the tolerance.

2 Results and Discussion

2.1 Experimental data

The burden descending experiment was conducted by Ichida et al.[17] using a three-dimensional semicircular 1/20 scaled model under thermal state. Coke and quasi-ore (low melting point metal) were charged layer by layer alternatively by the bell and movable armors (MA). Three charging patterns including C_0O_0 (MA not yet used), C_0O_{20} (charging ore closer to the furnace center) and $C_{20}O_0$ (charging coke closer to the furnace center) were used corresponding to different operating conditions. The reported data were used to validate four burden descent models in this work. Figs. 2(a) − 2(c) show the burden structure[17] of which the experimental descend-

(a) C_0O_0;   (b) C_0O_{20};   (c) $C_{20}O_0$.
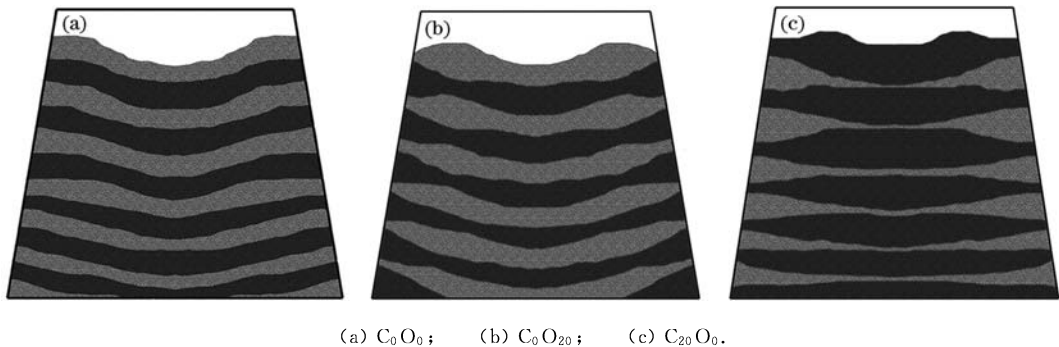
Fig. 2   Experimental burden structure in different charging patterns

ing condition reached almost the stationary state in different charging patterns. Figs. 3(a) − 3(c) show the experimental layer timelines[17] which are measured every other 10 min.

2.2 Parameter determination

The process analyzed in this study is a 1/20 scaled warm model of Tobata BF No.1, which has a

throat radius of 255 mm, shaft angle of 81°04′, belly diameter of 756 mm, belly height of 150 mm, bosh angle of 81°07′, and hearth diameter of 690 mm. The present study focuses on the burden flow in the shaft region, namely the area between the burden profile timelines of 0 and 30 min, as shown in Fig. 3. The burden descending volume in each time interval is calculated via integration as shown in Table 1.
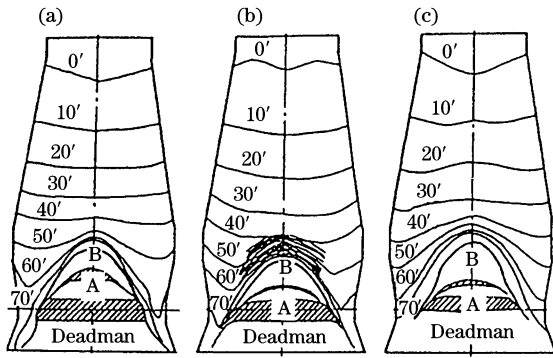
(a) $C_0 O_0$;   (b) $C_0 O_{20}$;   (c) $C_{20} O_0$.

Fig. 3   Experimental timeline layers in different charging patterns

Table 1   Burden descending volume in each time interval   m³

Charging pattern	Descending volume		
	0—10 min	10—20 min	20—30 min
$C_0 O_0$	0.059 60	0.053 43	0.047 02
$C_0 O_{20}$	0.074 89	0.061 29	0.061 48
$C_{20} O_0$	0.061 89	0.067 59	0.056 88
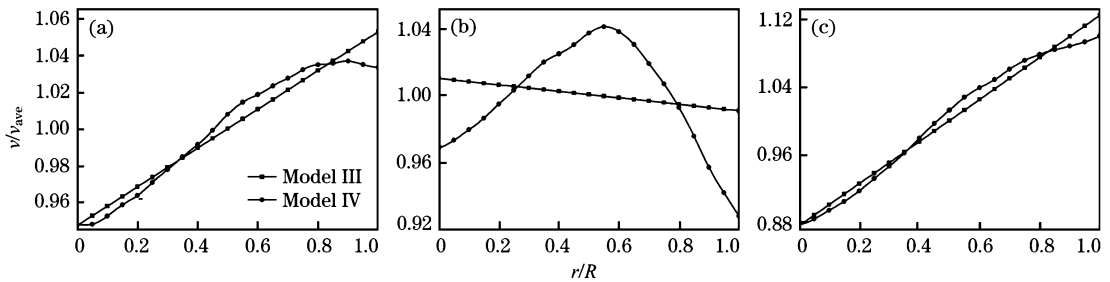
(a) $C_0 O_0$;   (b) $C_0 O_{20}$;   (c) $C_{20} O_0$.

Fig. 4   Normalized descending velocity distribution in different charging patterns

As the determination of the parameter X in Model II was not involved in Kajiwara's research[16], an exhaustion method was utilized to determine the optimal X in this study. X ranges from 0 to $0.9R$ with an increment of $0.1R$, and the corresponding modeled burden structures are analyzed combined with experimental data. As a result, optimal X with minimum error are determined as $0.3R$, 0 and $0.3R$ in charging pattern $C_0 O_0$, $C_0 O_{20}$ and $C_{20} O_0$, respectively.

In Model IV, the normalized descending velocity distribution of the top layer, which can be measured entirely and accurately by field equipments such as laser scanner and multiradar, is approximately represented by the normalized descending distance between the top adjacent layers (Fig. 2) along the assumed particle path. The corresponding results in different charging patterns are shown in Fig. 4, where, v/v_{ave} represents the normalized descending velocity; v and v_{ave} are particle's descending velocity and averaged descending velocity along the radial di-

rection, respectively, m/s; r/R represents the normalized radius; and r is the distance between a specific particle and the furnace centerline, m.

As for Model III, with the combination of the entire descending velocity distribution data in Model IV, parameters like k and c in each charging pattern are determined via least square estimation (LSE) method and listed in Table 2.

Table 2   Input parameters in Model III

Charging pattern	k	c
$C_0 O_0$	0.105 6	0.947 2
$C_0 O_{20}$	−0.192 2	1.010 0
$C_{20} O_0$	0.249 0	0.875 5

2.3   Evaluation of burden descent models

### 2.3.1   *Comparison of burden structures modeled by different descent models*

The initial profile specified for the simulation is identical with the previous stockline profile obtained by the experiment[5]. The development of the stockline profile along each time interval is calculated by different burden descent models and the corresponding measured profiles in different charging patterns are shown in Figs. 5—7.

For charging pattern $C_0 O_0$ (Fig. 5), it is clear that burden profiles in each modeled result are in good agreement with the experimental measurements. The similarity between different modeled burden profiles is mainly caused by the quasi-steady radial descending velocity distribution (Fig. 4(a)). The descending velocity in charging pattern $C_0 O_0$ rises slightly with increasing r/R. Compared with the average descending velocity, the maximum relative velocity difference value along the radial direction is only about 5%, which is such a slight difference that different burden descent models perform approximately the same burden descending distance along the
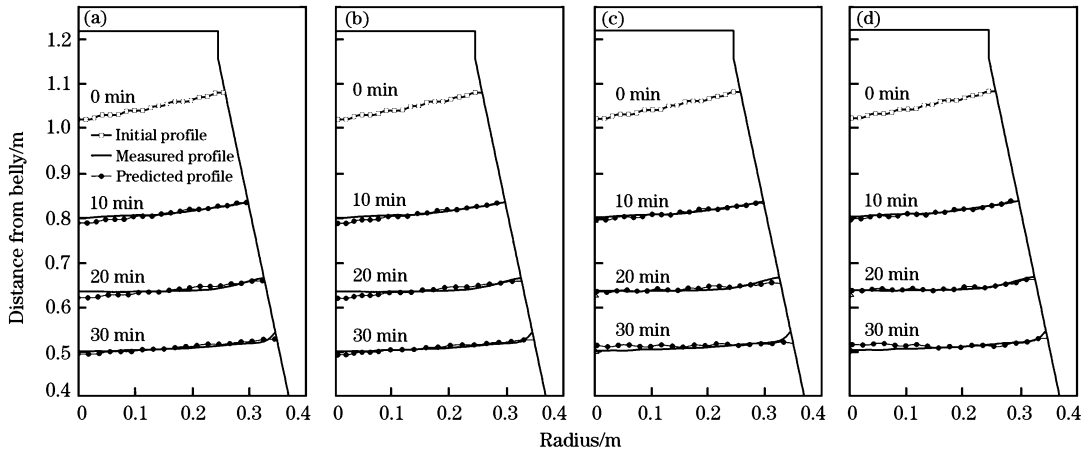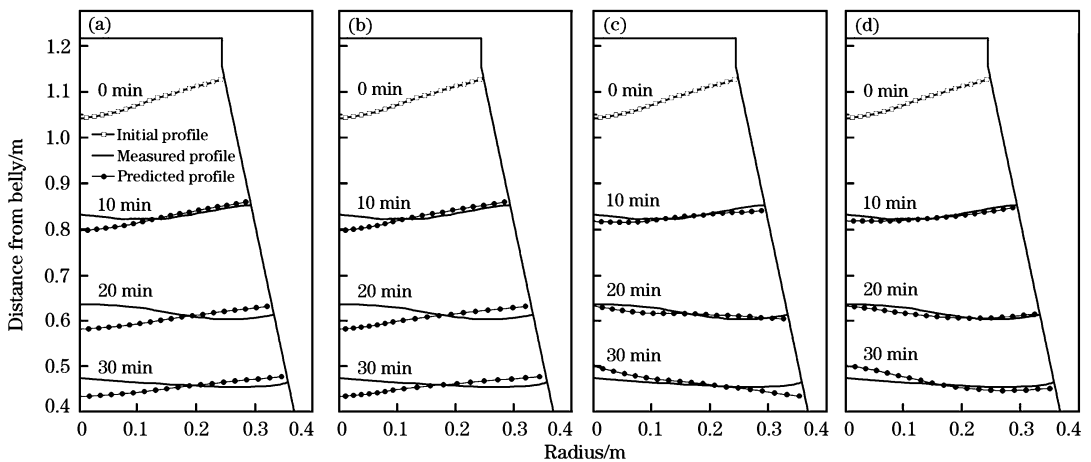
(a) Model I;   (b) Model II;   (c) Model III;   (d) Model IV.

Fig. 5   Comparison between calculated results and experimental data with charging pattern $C_0 O_0$
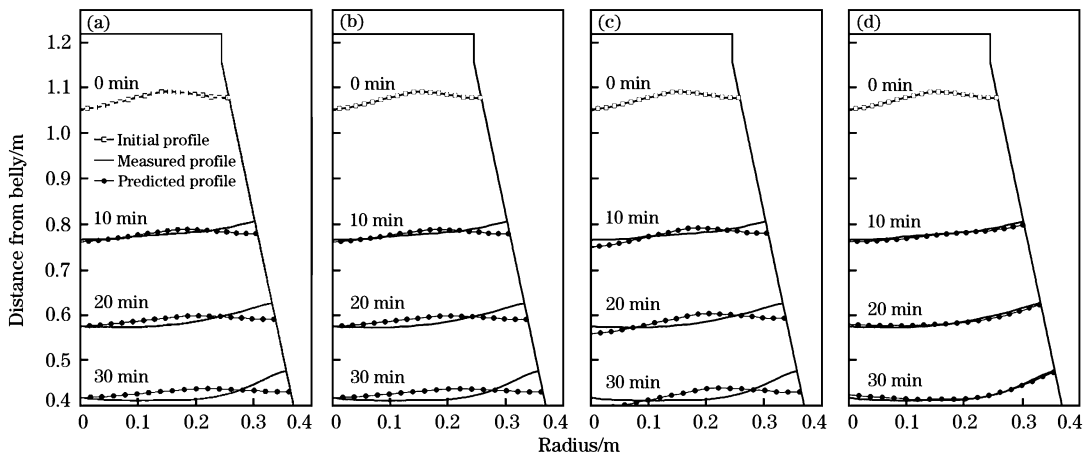
(a) Model I;   (b) Model II;   (c) Model III;   (d) Model IV.

Fig. 6   Comparison between calculated results and experimental data with charging pattern $C_0 O_{20}$

(a) Model I;   (b) Model II;   (c) Model III;   (d) Model IV.

Fig. 7   Comparison between calculated results and experimental data with charging pattern $C_{20} O_0$

radial direction. This result means that burden descending process with quasi-steady descending velocity distribution can be accurately calculated by all the four burden descent models.

The same burden profile for charging pattern $C_0 O_{20}$ are shown in Fig. 6. Compared with the exper-

iment performed by Ichida et al.[15], Model IV shows the best agreement, while the other three models exhibit considerable deviations in the middle and peripheral region. As shown in Fig. 4(b), the burden descending velocity in the charging pattern $C_0 O_{20}$ presents an unstable tendency along the radial direction in which the burden descending velocity increases slowly in the beginning, but decreases dramatically later. This may be the reason that caused considerable discrepancy between modeled and measured results in the middle and peripheral region in the other three models.

Fig. 7 shows the same burden profile for charging pattern $C_{20} O_0$. Comparing the calculation presented in the four subfigures, the results modeled by Model III and Model IV must be considered very consistent with the experimental result, despite some small deviations in the centre region. The results for Model I and Model II are acceptable in the peripheral region, but deviate strongly in the centre region from the experimental findings. These results are mainly caused by the linear velocity distribution as shown in Fig. 4(c).

2.3.2 Relative error between experimental and modeled results

To quantitatively evaluate the error between the experimental and calculated results, the area between measured and predicted profiles was divided into several quadrangles composed of four dots as shown in Fig. 8. The burden profiles in Fig. 8 were chosen from the calculated result in Model I and experimental data in the timeline of 20 min with the charging pattern of $C_{20} O_0$. The area between measured and predicted profiles can be calculated using the sum of a_i, and a_i can be estimated by Eqs. (5) and (6).

$$h_i = (|y_{E,i+1} - y_{M,i+1}| + |y_{E,i} - y_{M,i}|)/2 \quad (5)$$
$$a_i = h_i \cdot (x_{i+1} - x_i) \quad (6)$$

where, h_i represents the height of the ith quadrangle,

Fig. 8 Calculation of stock layer area divided by several quadrangles

m; a_i is the area of the ith quadrangle, m²; x_i is the horizontal distance of the ith point of the burden profile, m; and $y_{E,i}$, $y_{M,i}$, $y_{E,i+1}$, $y_{M,i+1}$ represent the vertical distance of the ith and $(i+1)$th point in the model and experimental results, respectively, m.

In Fig. 9, a_i was converted to the volume of a ring, V_i, by axial rotation. V_i and the total volume surrounded by measured and predicted profiles, V_n, were calculated using Eqs. (7)−(9).

$$r_i = (x_{i+1} + x_i)/2 \quad (7)$$
$$V_i = 2\pi r_i a_i \quad (8)$$
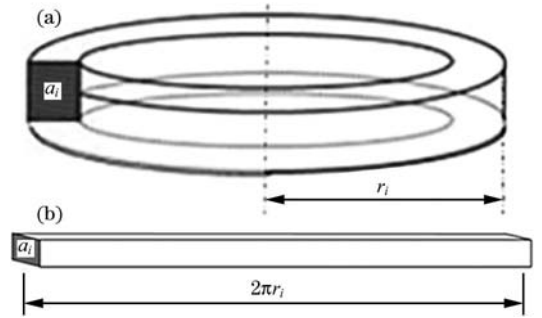$$V_n = \sum_1^N V_i \quad (9)$$

Fig. 9 Method to convert area into volume

The evaluation error is calculated as follows:

$$\text{Error} = \frac{V_n}{V_{\text{batch}}} = \sum_{i=1}^N \frac{\pi}{2} (x_{i+1} - x_i)(x_{i+1} + x_i)$$
$$(|y_{E,i+1} - y_{M,i+1}| + |y_{E,i} - y_{M,i}|)/V_{\text{batch}} \quad (10)$$

where, V_n represents the volume enclosed by the discrepancy between the calculated and measured burden profile in each timeline, m³; V_{batch} is the total batch volume (containing coke batch and ore batch) in one charging pattern, m³; and N is the total number of the points among the individual profile. Thus, Error is expressed as V_n normalized by the total batch volume V_{batch}. It should be noted that the value of N greatly affects the calculation accuracy of V_n. In the previous research performed by Park et al.[4,5], N was set as 141, whereas in the present work, N is increased to 201 so as to assure satisfactory precision. The Error values of each models in each charging pattern are shown in Fig. 10. Error of Model I in charging pattern $C_0 O_{20}$ is not mentioned in Fig. 10(b) since the result is essentially the same to that in Model II when X is equal to 0.

It is clear that Model IV has the minimum error especially in charging pattern $C_0 O_{20}$, where the quantitative error of each timeline is less than 10% while the other three models reach the maximum error of
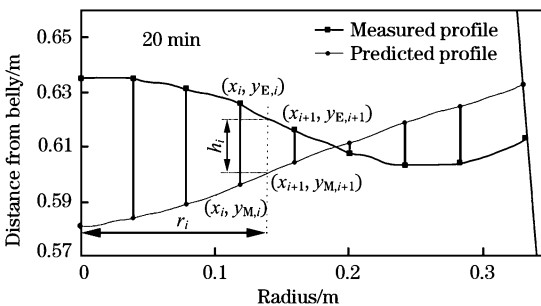
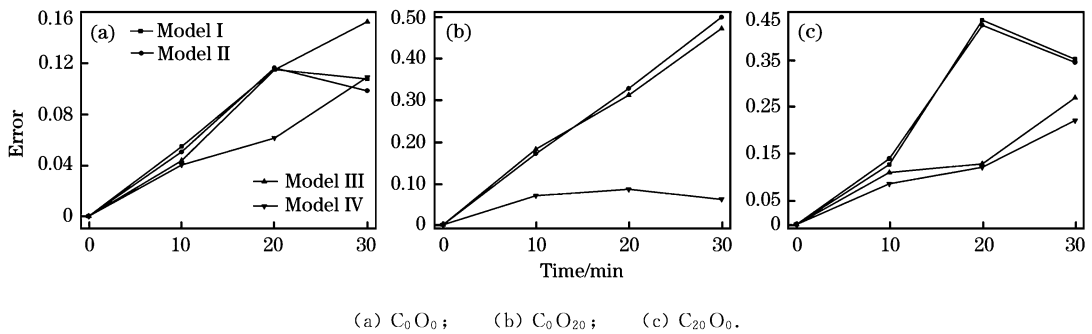(a) C_0O_0;   (b) C_0O_{20};   (c) $C_{20}O_0$.

Fig. 10   Error of each model in different charging patterns

approximately 50% in the 30 min timeline. Besides, Model III may also be desirable to model the burden descending process when the burden descending velocity presents a linear tend along the radial direction. In Fig. 10(c), Error of Model III in the 20 min timeline is only about 10%, whereas in Model I and Model II, the corresponding Error increased to 42%, which may significantly reduce the accuracy of the calculated gas flow in the shaft region.

As for rough predicting, Model I and Model II may also be advisable since both of them caught the main profile of the burden structure especially in charging pattern C_0O_0. Considering the complex work to determine the optimum X and the inconspicuous advantage of Model II, Model I might be the first option for rough burden structure predicting.

In addition, an upward tendency of Error is witnessed by all charging patterns with increasing timeline. This phenomenon is believed to be caused by the deadman formation in the lower part of BF (Fig. 3), which may significantly influence the radial velocity distribution tendency in descending process.

3   Conclusions

（1）Burden descending process with quasi-steady descending velocity distribution can be accurately calculated by all the four burden descent models.

（2）Model IV shows the highest level of precision especially when burden descends with unstable velocity distribution tendency.

（3）Model III may be desirable to model the burden descending process when the burden descending velocity presents a linear tendency.

（4）Model I might be the first option for rough burden structure prediction.

References:

[1]   K. Yang, S. Choi, J. Chung, J. Yagi, ISIJ Int. 50 (2010) 972-980.

[2]   J. Jiménez, J. Mochon, A. Formoso, J. S. D. Ayala, ISIJ Int. 40 (2000) 114-120.

[3]   J. Jiménez, J. Mochon, J. S. D. Ayala, ISIJ Int. 44 (2004) 518-526.

[4]   J. I. Park, H. J. Jung, M. K. Jo, H. S. Oh, J. W. Han, Met. Mater. Int. 17 (2011) 485-496.

[5]   J. I. Park, U. H. Bark, K. S. Jang, H. S. Oh, J. W. Han, ISIJ Int. 51 (2011) 1617-1623.

[6]   P. Y. Shi, D. Fu, P. Zhou, C. Q. Zhou, Ironmak. Steelmak. 42 (2015) 756-762.

[7]   V. R. Radhakrishnan, K. M. Ram, J. Process Control 11 (2001) 565-586.

[8]   H. Mio, S. Komatsuki, M. Akashi, A. Shimosaka, Y. Shirakawa, J. Hidaka, M. Kadowaki, S. Matsuzaki, K. Kunitomo, ISIJ Int. 48 (2008) 1696-1703.

[9]   D. Fu, F. Huang, F. Tian, C. Q. Zhou, in: AISTech 2010 Proceedings, Vol. 1, AISTech, Pittsburgh, PA, 2010, pp. 693-700.

[10]   Y. Kajiwara, T. Inada, T. Tanaka, Trans. ISIJ 28 (1988) 916-925.

[11]   M. Hattori, B. Iino, A. Shimomura, H. Tsukiji, T. Ariyama, ISIJ Int. 33 (1993) 1070-1077.

[12]   Z. J. Teng, S. S. Cheng, P. Y. Du, X. B. Guo, Int. J. Miner. Metall. Mater. 20 (2013) 620-626.

[13]   T. Mitra, H. Saxén, Metall. Mater. Trans. B 45 (2014) 2382-2394.

[14]   H. Nishio, T. Ariyama, Tetsu-to-Hagane 68 (1982) 2330-2337.

[15]   M. Ichida, M. Takao, K. Kunitomo, S. Matsuzaki, T. Deno, K. Nishihara, ISIJ Int. 36 (1996) 493-502.

[16]   Y. Kajiwara, T. Jimbo, T. Sakai, Trans. ISIJ 23 (1983) 1045-1052.

[17]   M. Ichida, K. Nishihara, K. Tamura, M. Sugata, H. Ono, ISIJ Int. 31 (1991) 505-514.

[18]   X. Z. Chen, J. D. Wei, D. Xu, Q. W. Hou, Z. L. Bai, ISIJ Int. 52 (2012) 2048-2054.

[19]   D. Fu, F. Tian, G. Chen, D. F. Huang, C. Q. Zhou, in: ASME 2009 Heat Transfer Summer Conference Collocated with the InterPACK09 and 3rd Energy Sustainability Conferences, American Society of Mechanical Engineers, San Francisco, 2009, pp. 797-805.

[20]   J. Xu, S. L. Wu, M. Y. Kou, L. H. Zhang, X. B. Yu, Appl. Math. Model. 35 (2011) 1439-1455.

[21]   T. Ren, J. Zhao, C. S. Qiao, H. Zhao, M. Zheng, Iron and Steel 33 (1998) No. 5, 9-12.